AIRCRAFT INDUCED DRAG MINIMIZATION USING A CONSTRAINED OPTIMIZATION METHOD

André Luiz Martins
Aircraft Laboratory - USP - Brazil

Renato Silva Ribeiro
Empresa Brasileira de Aeronáutica - EMBRAER - Brazil

ABSTRACT

A constrained optimization method for lifting surfaces configurations has been developed. The method consists of a 3D vortex lattice method coupled to a numeric function optimizer algorithm. It has been applied in a case study for induced drag reduction of a medium range transport aircraft in cruise conditions, by suitable shaping of spanwise wing local incidence distribution (torsion). Design constraints for trimmed cruise flight and stall inception safety have been introduced progressively, generating different constraint severity level optimization cases. The method was successful in producing optimum configurations wich respected the required constraints for each case. Also, the results enabled to stablish the relative merits of each constraint adopted, indicating that the method have been able to follow known, phisically correct trends.

List of Symbols

x, y, z	Reference coordinate system (Fig. 4)
g	Gravity acceleration (9.81 m/s^2);
m	Aicraft mass (kg);
ρ	Air density (kg/m^3);
U_∞	Freestream flow velocity (m/s);
M	Mach number;
b	Wing span (m);
mac	Mean aerodynamic chord (m);
c(y)	Spanwise chord distribution (m);
y_s	Stall inception spanwise coordinate;
y_{safe}	Stall safety limit spanwise coordinate;
S	Reference area (projected wing area - m^2);
CG	Center of gravity;
α	Aircraft angle of attack (degrees);
w_1	Wing tip local incidence angle (degrees);
w_2	Wing break local incidence angle (degrees);
i_h	Horizontal stabilizer incidence angle (deg);
L	lift force (N);
Di	induced drag force (N);
C_L	Lift coefficient;
C_{Di}	Induced drag coefficient;
CM	Pitching moment coefficient;
l(y)	Spanwise adimensional lift distribution;
c_l(y)	Spanwise lift coefficient distribution;
c_{lb}(y)	Spanwise basic lift coefficient distribution;
c_{la}(y)	Spanwise additional lift coefficient distrib.;
$\{X_i\}$	Optimization decision variables set;
$F(\{X_i\})$	Optimization objective function;
$\{G_i\}$	Constraint functions set;
[AIC]	Aerodynamic influence coefficient matrix;
[RHS]	Contour conditions vector;
$[K_i]$	Vortex intensity vector.

Subscripts

max	maximum;
opt	optimum;
cruise	cruise condition reference.

Introduction

In general engineering practice, two basic distinct problems are usual: analisys and design. In the field of aircraft aerodynamics, this distinction is of special importance: the objective of analisys is to evaluate the aerodynamic characteristics of a given configuration. Conversely, the design process searches for the configuration wich is aerodynamically best suited for an specific mission and, at the same time, respects the constraints imposed by other design needs (structure, weight, operational feasability, etc.).

In aircraft design, the use of any "traditional" standard or configuration does not necessarily brings good results promptly. Currently, constant design research has become the key for survival within the constantly changing aeronautical market. On the other hand, aircraft design optimization is an specially complicated task, due to the immense number of design variables and constraints involved.

The last three decades brougth a quantum leap in aerodynamic analisys methods, due to the crescent availability of computer power. In spite of that, computational design methods did not present such growth. As a result, until recent years, powerful and sofisticated computational analisys methods, capable of treating large numbers of design variables, have been used in "manual, cut and try" design methodologies. Within that context, recent advances[1] have been made in order to develop viable computational *design* tools, able to control design variables and constraints in search for

optimum configurations, given conditions and background imposed by previous experience.

Based on these facts, a constrained direct optimization method for the geometry of aircraft lifting surfaces has been formulated, based on a three dimensional vortex lattice analisys method coupled to a numerical multivariable function optimizer. Tests and validations have been performed around the problem of induced drag minimization for a medium range transport aicraft, in cruise condition, by applying suitable wing torsion. The effects of different design constraints on induced drag have been evaluated.

Description of the Method

Constrained direct optimization is one of the current basic trends[1] in computational design methods. The technique is based in coupling a desired analisys method to a numerical multivariable function optimizer routine. The optimizer is able to use the analisys method as a multivariable function evaluator, in wich a chosen objective aerodynamic characteristic F (for example, induced drag) is dependent of a given set of decision variables $\{X_i\}$ (for example, geometric characteristics). The routine is then able to numerically search for the set of decision variables values $\{X_i\}_{opt}$ wich returns the minimum (or maximum) value of the objective aerodynamic characteristic chosen $F(\{X_i\}_{opt})$, in an iterative process of analisys and evaluation (Figure 1). The final set of decision variables must be constrained to a certain domain, to ensure that the final result is feasible for the mission in mind.

In this work, a vortex lattice method was chosen to perform aerodynamic analisys and has been coupled to an extensively tested function minimization method[3]. Both methods are described below.

In comparision to the so called "inverse design" methods, direct optimization is a more general approach, once no "desired optimum" must be prescribed to be reached. Such desired optimum is a natural result of the variable set search. One of the disavantages of the method is its larger computer cost (run time) reached if too many decision variables are desired and/or the analisys method consumes too much processing time, as it is the case of highly discretized and detailed CFD models. In spite of that, a future growth of direct optimization usage can be previewed along the current growth in computer power availability.

Vortex Lattice Analisys Method: VORLAT algorithm.

The vortex lattice analisys method[3] is a numerical solution of the lifting surface theory equations[4] for inviscid potential flow. The real lifting surfaces are aproximated by a set of trapezoidal planar elements, with no thickness taken into account (Figure 1). Through Green's third identity, the Laplace's equation wich represents the potential flow around the lifting surfaces can be expressed as a combination of singularities over the planar surfaces. In this case, the trapezoidal planar elements model is discretized in rectangular panels, each of them associated with a rectangular vortex ring of unknown intensity. The vortex trailing wake shed from the surfaces is modelled by horseshoe shaped semi-infinite vortices (in the plane of the elements), whose intensities satisfy the Kutta condition at the trailing edge. As a numerical solution of the integral equation resultant from the singularities (vortices) distribution representation, mutual influence between the vortex panels is evaluated. This evaluation, associated with the contour condition of no flow penetration on representative control points on the panels, gives rise to a linear sistem of equations of the form:

$$[AIC][K_i] = [RHS] \qquad (1),$$

in wich $[K_i]$ is the solution vector for the vortex rings intensities. The aplication of the Kutta-Joukowski law to each vortex ring segment normal to the flow and the sum of the whole vortex rings effects gives total lift and induced drag forces, as well as total pitching moment and spanwise lift distributions.

In this approach, small angle chordwise camber and spanwise local incidence distributions can be taken into account by a simple linear contour conditions modification, wich affect the [RHS] vector. Also, a Prandtl-Glauert linear correction for compressibility[4] in subsonic flight has been implemented. The resulting VORLAT algorithm has been extensively validated by comparision with classic lifting surface solutions[4], and its convergence with crescent panel discretization was satisfatory[5].

The Vortex Lattice method (VLM), although less sophisticated than higher order panel methods, is capable of great prediction accuracy for global forces and lift distributions of free lifting surfaces. It is very adequate for preliminary design needs and has low computational cost, reasons that make it ideal for a first implementation of a usable iterative optimization method.

Iterative Optimization Method: CONMIN algorithm.

An already validated numerical function minimization algorithm has been used. The CONMIN algorithm has

been implemented by G. N. Vanderplaats[2] in 1973. It is based on a gradient search method and has special features in order to identify and avoid local minimum values of the objective function $F(\{X_i\})$, ensuring that an absolute minimum $\{X_i\}_{opt}$ can be found. The algorithm settings can be adjusted for each aplication need, based on the function linearity degree and final result precision level desired. The number of decision variables to wich the method can be applied is limited only by the computer power available.

Constraint limits to the minimization search can be stablished in two ways. The first one is with *side constraints*, wich define the range of values a certain decision variable X_i can have. The second option is by applying *inequality constraints* that define a certain dominium range within the variables range by the imposition of inequations involving user-defined functions G_j. This inequations are of the form:

$$G_j \leq 0 \qquad (2)$$

The algorithm has been adopted due to its validated robustness for different applications and its availability. Any attempts of modification or deep interpretation of the gradient search method itself have been considered beyond the scope of this work. For further considerations on the method, the correspondent NASA technical memorandum[2] is recommended.

Optimization Method: VORLAT/CONMIN system.

The coupling between the VORLAT analisys algorithm and the CONMIN function optimizer has been made by common memory sharing between the variables involved and a simple interface routine able to translate the data between both algorithms (Figure 1). The CONMIN algorithm control variables and tolerances have been adjusted with basic first running tests[5], in wich the optimization iterative cycle has been started with different arbitrary initial values for the decision variables set {Xi}. The adjustment process enabled a final results precision up to 10^{-5} the values of the decision variables.

Description of the Optimization Cases: Induced Drag Reduction.

As mentioned above, the resulting VORLAT/CONMIN optimization method has been applied to induced drag minimization of aircraft lifting surfaces. The design case of induced drag reduction for a medium range transport airplane in cruise regime was chosen. The basic configuration chosen to be optimized is shown in Figure 3. It is important to remmember that the method is general, and that this problem in particular was taken as a first study.

Geometric Optimization Variables

The choice of the geometrical characteristics to be optimized on the configuration has been based on three criteria:

- Reduction of induced drag for a given C_L is essentially achieved by lift distribution shaping. One way to accomplish that is by suitable spanwise local incidence distribution, or "wing torsion".

- Other major geometric characteristics (ex.: chord relations, aspect ratio, wing sweep angle) for the chosen configuration in particular have already been defined ("frozen") due to other design constraints (wave drag, required structure, etc.).

- During VLM analisys, spanwise local incidences are considered in the [RHS] vector. The [AIC] matrix is defined by other geometric features of the configuration and its decomposition demands relatively large processing time, during the solution procedure. If local wing incidences are chosen as the decision variables, the [AIC] matrix needs to be calculated only during the first iteration, making the optimization process faster. As a result, an earlier deeper insight on the method as a whole could be enabled.

From these criteria, the geometric decision variables chosen are shown in Figure 4 and are described as follows:

(a) α (Alpha): aircraft angle of attack, measured between wing root and freestream velocity U_∞.
(b) w_1: local wing incidence angle at the wing tip, relative to wing root.
(c) w_2: local wing incidence angle at the wing discontinuity, relative to wing root.
(d) i_h: horizontal stabilizer incidence angle, relative to wing root.

(NOTE: local incidences are measured from the the zero lift line of the local surface airfoil)

For the local incidence angle distributions, VORLAT considers linear variation along the span of each trapezoidal element. Figure 5 shows the vortex lattice model of the configuration. No attempt has been made to model the fuselage effects by any methods in this preliminary work.

Constraints Definition

The condition of an aircraft in cruise is characterized by its null translational and rotational aceleration. Given that conditions, the following can be written:

$$\sum F_Z = 0 \Rightarrow C_{L(cruise)} = \frac{mg}{\frac{1}{2}\rho U_\infty^2 S} \qquad (3)$$

$$\sum M_{y(CG)} = 0 \Rightarrow C_{M(CG)} = 0$$

From Eqs. (3) it can be stablished that for a tipical operational aircraft weight, a tipical cruise C_L *must* be sustained. Also, the cruise moment coefficient around the CG *must* be zero. These two conditions are the first two design constraints to be imposed during the optimization. They are also the reason to choose both α and $\mathbf{i_h}$ as decision variables.

In this work, another constraint of interest has been envisaged, to evaluate the ability of the method to follow known trends. It can be required from the method that the final optimized configuration also assures a safe stall inception. To evaluate the trend of stall progression, the classical method[6] of extrapolation of the spanwise lift coefficient distribution $c_l(y)$ to C_{Lmax} has been used. In that method, the $c_l(y)$ distribution is assumed to have a linear relation wit C_L, even near the stall angle of attack, of the form:

$$c_l(y) = c_{lb}(y) + C_L c_{la}(y) \qquad (4)$$

From that point it can also be stated that the stall spanwise starting point is that for wich the local lift coefficient $c_l(y)$ first reaches the local maximum profile lift coefficient $c_{lpmax}(y)$. From this statement and Eq. (4), the following can be written:

$$C_{Lmax} = min\left(\frac{c_{lpmax}(y) - c_{lb}(y)}{c_{la}(y)}\right) \qquad (5)$$

The spanwise stall station y_s can be estimated as that for wich the minimum in Eq. (5) occurs. Although seemingly crude, this estimation of y_s can be very precise for high aspect ratio surfaces[6], using the linear results from VORLAT, and is sufficient within the scope of this work.

A tipical preliminary stall safety constraint is to limit y_s to a certain semi-span range inboard from a defined safe position y_{safe}, to ensure that stall separation regions do not spoil the ailerons region and eventually cause loss of roll control during slow speed manouvering. This constraint could be written as:

$$y_s < y_{safe} \qquad (6)$$

The three constraints described above had to be represented by inequations involving the G_i functions described above. The three constraints then have been defined by:

$$G_1 = C_{L(cruise)} - C_L \leq 0 \qquad (7a)$$

$$G_2 = 0 - C_{M(CG)} \leq 0 \qquad (7b)$$

$$G_3 = y_{safe} - y_s \leq 0 \qquad (7c)$$

From inequation (7a) it can be seen that C_L values greater than $C_{L(cruise)}$ are allowed, what could represent a possibility outside the constraint requirement (C_L = $C_{L(cruise)}$). The logic for this inequation adoption is that, if the method is searching for minimum C_{Di}, it will search for the minimum C_L possible within the constraint boundaries, that is, C_L = $C_{L(cruise)}$. That is a natural consequence, once C_{Di} is proportional to $(C_L)^2$. The same logic can be followed for inequation (7b), wich ensures $C_{M(CG)} = 0$.

For the configuration under study, the following values were used:

$$C_{L(cruise)} = 0.3 \qquad (8)$$

$$y_{safe} = 0.63\ b/2$$

$$M_{(cruise)} = 0.6$$

The value for ysafe was taken as the spanwise position of the inboard end of the aileron (Figure 3). The $c_{lpmax}(y)$ local maximum airfoil lift coefficient distribution estimation (based on information from theoriginal configuration designer) can be given by:

$$0 \leq y/(b/2) \leq 0.382 \Rightarrow c_{lpmax}(y) = 1.6 + 0.5236y/(b/2); \qquad (9.a)$$

$$0.382 \leq y/(b/2) \leq 1 \Rightarrow c_{lpmax}(y) = 1.8 \qquad (9.b)$$

Definition of Optimization Cases

Once the method has been implemented and tested, it has not been considered of interest to introduce all variables and constraints described above at once. Intermediary optimization cases have been defined by progressive introduction of variables and constraints, so that the relative effects of each one of them on the final optimized result could be appreciated.

For the optimization variables, it has been first considered that a continuous local incidence distribution could be adopted along the whole semi-span; in this case, w_2 would always be proportional to w_1. The other option was to consider the possibility of a w_2 angle independent of w_1 and defining, in general, a local incidence distribution discontinuity at the wing break (Figure 3).

For the optimization constraints, the alternatives of trimmed ($C_{M(CG)} = 0$) and not trimmed final results have been considered of interest in evaluating the influence of trimming on minimum induced drag. Also, the influence of the adoption of the stall safety constraint (or not) has been considered of interest, once both stall inception

spanwise location and induced drag are directly dependent on the lift distribution shape.

Table 1 sinthetizes all intermediary cases devised for optimization, given diferent levels of variables and constraints adoption. The designation suffixes 1 and 2 correspond to the continuous local incidence distribution (w_2 dependent of w_1) and to independent w_1 and w_2 local angles, respectively (Figure 4).

It is important to note that the decision variables α and i_h are independent in all optimization cases, except for the value $i_h = 0$ for the not trimmed cases.

Results

The final optimization results for both geometric decision variables and aerodynamic coefficients is presented in Table 2, for all optimization cases stablished above.

Figure 6 shows the resulting optimized local incidence angle for the main wing for all the cases with continuous local incidence (suffix 1). Figure 7 shows the same distributions for the other cases, with w_1 and w_2 as independent variables (suffix 2).

Figure 8 presents an overall comparision of minimum C_{Di} values obtained for each optimization case. Figure 9 brings a percentual comparision in terms of minimum C_{Di} variations among the results, in relation to the minimum value obtained (case C-2).

Analisys of the Results

One first observation that can be made from the results (Table 2) is that all design constraints imposed are satisfied for every optimization case performed. It is secondly observed that the less intense minimum C_{Di} among all cases was obtained for the case C-2. That has been expected, once this case does not satisfy the trimming and stall constraints and it is also free to manipulate both w_1 and w_2 independently. In spite of that, the minimum *useful* C_{Di} was obtained for CT-2, wich guarantees cruise trimming and presents a 5.39% greater C_{Di} relative to the not trimmed case C-2 (Figure 9).

Effects of stall safety constraint

It is observed that the stall constraints were satisfied at their limits, or $y_s = y_{safe}$. From Figure 6 it can be promptly noted that the introduction of the stall safety constraint causes a strong negative wingtip incidence w_1 for the cases with continuos variation of local incidence angle. This can be explained by the need, imposed by the constraint, to diminish wingtip $c_l(y)$ intensities in relation to inner stations of the wing, to move the stall inception point inboard. The same trend can be observed in Figure 7 for the other cases (w_2 independent of w_1), but here the $c_l(y)$ redistribution can be made with a more equilibrate final result, by also increasing w_2. Figures 8 and 9 indicate that both solutions increase C_{Di} significantly in relation to the minimum value obtained, although independent w_1 and w_2 angles caused less than half the increase observed with continuous distributions (17.1% against 43.1%).

Effects of the trimmed flight constraint

Figure 10 presents a C_{Di} percentual comparision between trimmed and not trimmed cases. From the data obtained it can be concluded that for the cases without stall safety constraint, the C_{Di} contribution due to trimming is 5.4% the value for the not trimmed condition.

On the other hand, when the stall constraint is introduced, the contribution is less significative. This is caused by the tendency to wingtip negative incidences in these cases (Figures 6 and 7). This effect, on a swept wing, reduces the zero lift moment coeficient negative intensity ("flying wing" effect), reducing the horizontal tail load and its contribution to induced drag.

Spanwise lift and lift coefficient distributions

Figure 11 shows adimensional lift distributions in the form $l(y) = c_l(y)c(y)/(C_L\ MAC)$, for $C_L = C_{L(cruise)}$. Figure 12 presents the respective $c_l(y)$ distributions, for M= 0 and $C_L = C_{Lmax}$. Both graph sets are shown only for the trimmed cruise cases, wich are the ones of real practical interest.

From Figure 11 it can be observed that cases CT-1 and CT-2 are those whose lift distributions closer resemble an elliptical lift distribution, wich gives minimum C_{Di}. This explains why these two cases offer less cruise C_{Di} among the trimming constraint cases. Also, it can be observed that the extra degree of freedom obtained with an independent w_2 variation gives CT-2 a slightly better (closer to elliptical) lift distribution than CT-1. In spite of that, the differences are small enough to make C_{Di} only 0.016% greater for CT-1.

Also from Figure 11, it can be noted the intense $l(y)$ deformation caused by the stall safety constraint in cases CTS-1 and CTS-2, causing the large increases observed in C_{Di}. In addition, the greatest distribution deformation for case CTS-1 is evident, explaining its largest induced drag (Figure 8).

Figure 12 clearly shows the stall constraint effect on $c_l(y)$ distributions. Maximum $c_l(y)$ values for cases CST-1 and

CTS-2 occur at y stations much far from the wing tip than cases CT-1 and CT-2, causing the stall inception point to move inboard. It is evident that both the unrestricted stall cases would cause stall separation just over the aileron region, at a spanwise station of about y/(b/2) = 0.76.

Conclusion

From the results obtained it could be noted the optimization method proposed was able to give adequate results that were accurate within the limiting hipothesis of the analisys method chosen.

For the induced drag reduction problem, proposed for a medium range transport aircraft, it could be observed that the progressive introduction of more restrictive design constraints (namely trimmed cruise flight and stall safety condition) caused sistematic increases on the minimum induced drag C_{Di} obtained for each optimization case. Also, the adoption of a greater number of independent decision variables (increase in degrees of freedom) caused the expected trend of improving the optimum point, reducing the induced drag. For this case study in induced drag reduction, the following items summarize the conclusions reached:

(1) The greatest increases observed in optimum C_{Di} occurred when the stall safety constraint of limiting spanwise position of stall inception point has been introduced. Due to the pronounced wing sweep wich tends to determine high local lift coefficients near the wing tip (Figure 12), intense variations in local wing incidence (wing torsion) have been introduced by the optimization method to satisfy the constraint. These intense variations also caused excessive local lift distribution deformation (Figure 11) and the consequent high induced drag.

(2) The optimization process allowed the visualization of the relative magnitude in C_{Di} increase caused by flight trimming. This kind of notion is important as a base for new configurations studies made to reduce trim drag (three surface aircraft, for example).

(3) Although the adoption of independent local incidence w_2 (Figure 4) tends to reduce optimum induced drag, this reduction was only significative when the stall constraint was adopted. For free stall inception position, minimum induced drag obtained for independent w_1 and w_2 was only 0.016% lower than that for continuous spanwise torsion.

The main merits of the constrained direct optimization method experimented in this case study can be summarized as follows:

(4) The optimization process is automatic, making people involved in design free to analise the whole. The final results can give a faster and deeper insight on the most important aspects of the problem, once less important variables and relations are registered in algorithm form.

(5) The study has been able to give design constraint "sensibility", as in predicting the relative induced drag increase caused by trimming or in defining the relative merits in the adoption of more degrees of freedom. For example, the small difference observed in minimum induced drag between cases that used or not w_2 as an independent variable could affect future decisions for the aircraft manufacture process and/or structural design.

(5) The great mimimum induced drag increases obtained with the stall constraint demonstrated that the method is able to predict real, known trends. This is true because it is known that it is inviable to adopt wing torsion to limit spanwise stall position on a wing with pronouced sweep, being more interesting to control stall inception by other means (mainly by local airfoil maximum lift manipulation). From this result it can be extrapolated that, within the limits of the analisys method hipothesis, less known trends could be explored through computational optimization.

REFERENCES

[1] Dulikravitch, G.S.: "Aerodynamic Shape Design and Optimization: Status and Trends". *Journal of Aircraft,* Vol.29, No.6, Nov-Dez 1992. American Institute of Aeronautics and Astronautics, USA

[2] Vanderplaats, G. N.: *CONMIN - A FORTRAN Program for Contrained Function Minimization.* NASA Technical Memorandum X-62282, Ames Research Center, USA, 1973.

[3] Various authors, edited by. Morino, L: *Computational Methods in Potential Aerodynamics,* Ed. Springer-Verlag, Berlin, 1979.

[4] Schlichting, H. and Truckenbrodt, E.: *Aerodynamics of the Airplane,* Ed. McGraw Hill, USA, 1979;

[5] Martins, A.L. and Ribeiro, R.S.: Otimização de Asas por um Método de Malha de Vórtices. Student factory work period report. Author, 1994.

[6] Abbott, I.H. and Doenhoff, A.E.: *Theory of Wing Sections,* Ed. Dover, USA, 1959.

[7] Ribeiro, R. S.: *Analysis os Wing Wake Roll-Up Using a Vortex-in-Cell Method.* PhD Thesis. Stanford University, USA, 1992.

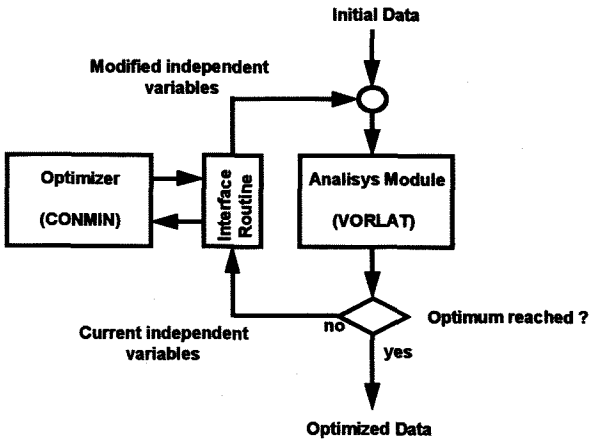

Figure 1 - Constrained direct optimization method

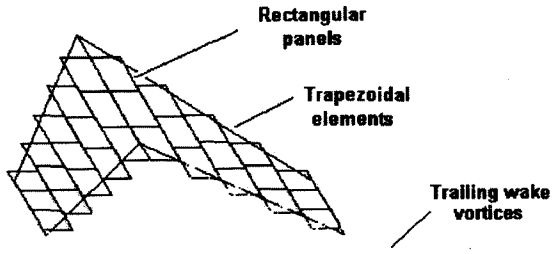

Figure 2 - Example vortex lattice model (swept wing, low discretization)

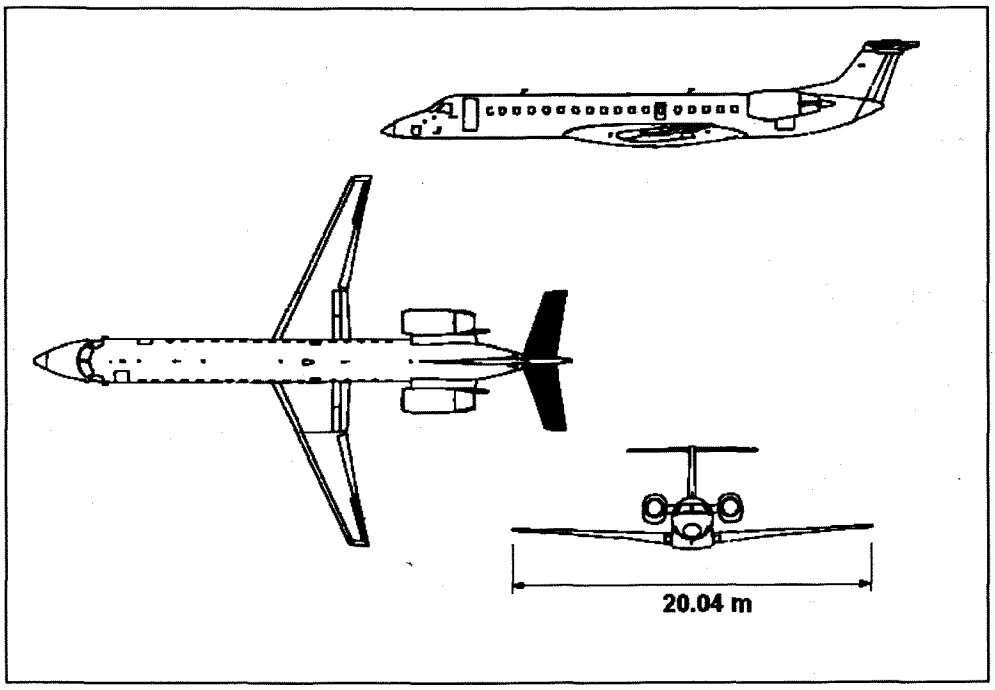

Figure 3 - Aircraft configuration for optimization case study.

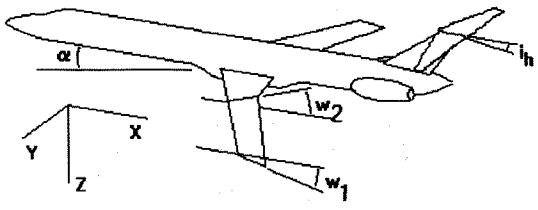

Figure 4 - Optimization geometric decision variables.

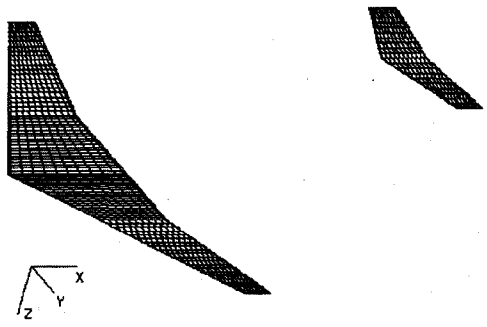

Figure 5 - Configuration vortex lattice model.

Not Stall Constrained Cases	Not trimmed		Trimmed ($C_{M(CG)}$ =0)	
	C-1	C-2	CT-1	CT-2
Optimized Variables:				
α (degrees)	3.0391	2.5861	3.4248	2.9645
w_2 (degrees)	0.6749	0.6801	0.0837	0.0993
w_1 (degrees)	0.2578 (*)	1.0972	0.0320 (*)	0.8822
i_h (degrees)	0.0 (*)	0.0 (*)	-3.2635	-2.8079
Aerodynamic Coefficients, Optimized				
10^4 C_{Di}	3.9051	3.8896	4.1155	4.0991
C_L	0.3000	0.3000	0.3000	0.3000
$C_{M(CG)}$	-0.0631	-0.0630	0.0000	0.0000
Stall Constrained Cases	**Vôo não trimado**		**Vôo trimado**	
	CS-1	**CS-2**	**CTS-1**	**CTS-2**
Optimized Variables:				
α (degrees)	6.0564	1.7132	6.1044	2.0612
w_2 (degrees)	-6.9248	-2.1858	-6.9232	-2.4412
w_1 (degrees)	-2.6453 (*)	3.7378	-2.6447 (*)	3.3956
i_h (degrees)	0.0 (*)	0.0 (*)	-5.1226	-1.6188
Aerodynamic Coefficients, Optimized				
10^4 C_{Di}	5.5334	4.4279	5.5667	4.5539
C_L	0.3000	0.3000	0.3000	0.3000
$C_{M(CG)}$	-0.0194	-0.0464	0.0000	0.0000
Ystall	0.6300	0.6300	0.6300	0.6300

Table 2 - Final optimization results.

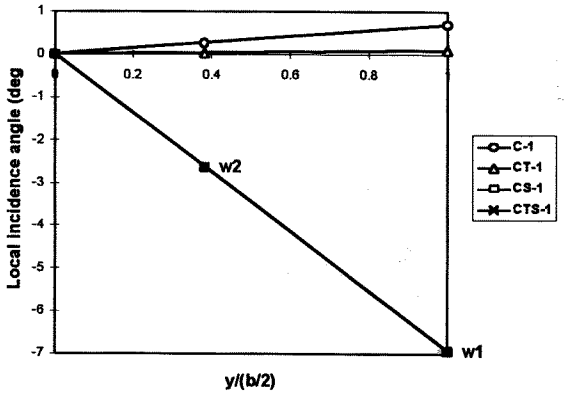

Figure 6 - Optimum local incidence, continuous distribution (w_2 = k w_1)

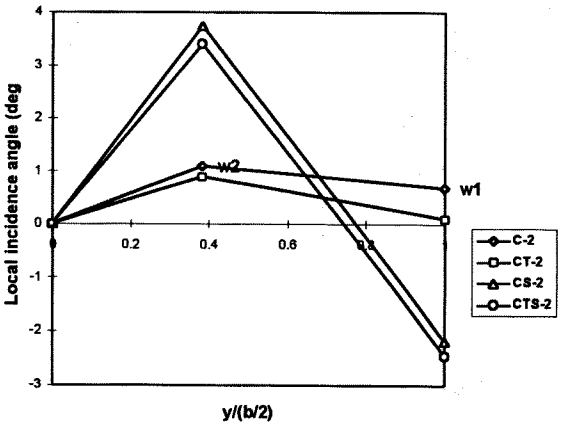

Figure 7 - Optimum local incidence angles distribution, independent w_1 and w_2.

	Not stall constrained	Stall constrained
Not trimmed cases	C-1	CS-1
	C-2	CS-2
Trimmed Cases	CT-1	CTS-1
	CT-2	CTS-2

Table 1 - Optimization cases.
(Suffix 1 ⇒ w_2 = kw_1 ; Suffix 2 ⇒ Independent w_2 and w_1)

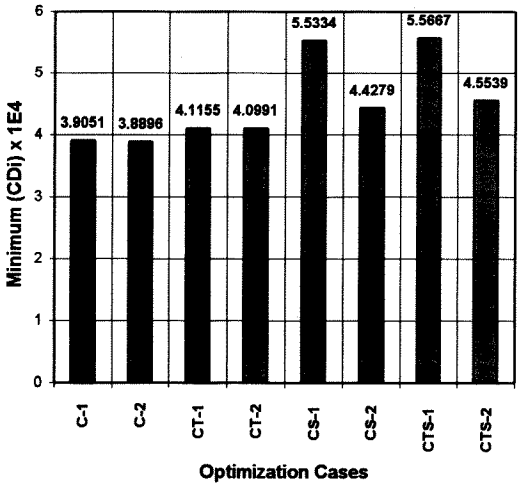

Figure 8 - Optimum (minimum) values obtained for (10^4) C_{Di}.

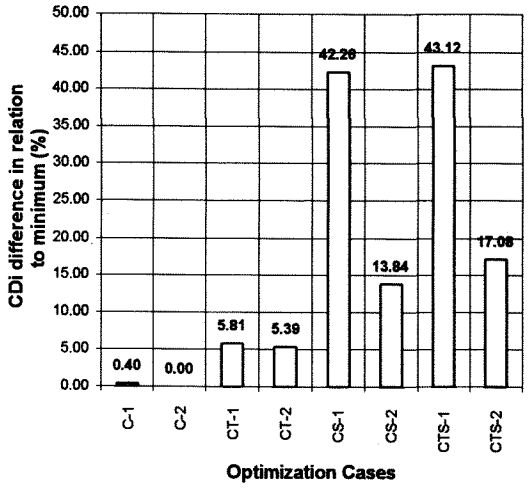

Figure 9 - Percentual C_{Di} diferences in relation to minimum (case C-2)

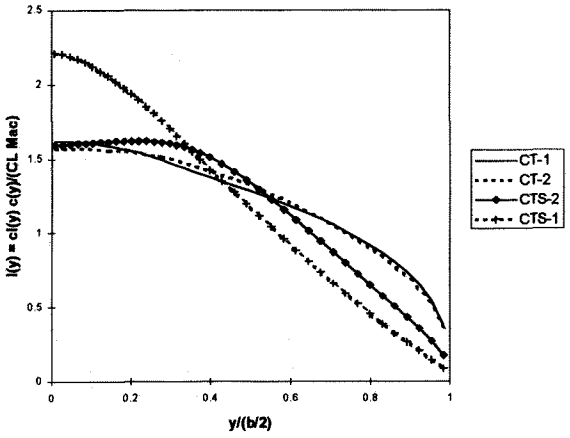

Figure 11 - Adimensional spanwise lift distributions, l(y) = c_l(y) c(y) /(C_L mac), trimmed cases, M = $M_{(cruise)}$.

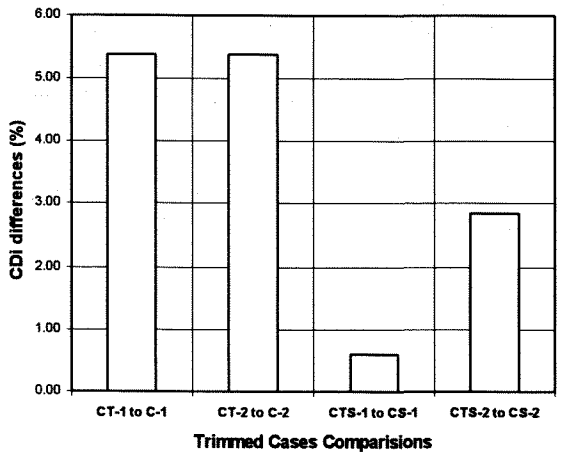

Figure 10 - Percentual variations in C_{Di} due to trim.

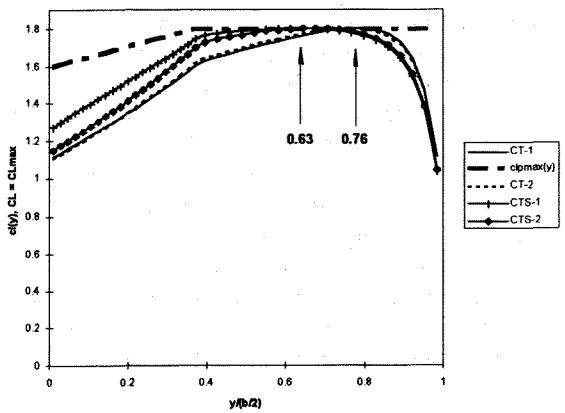

Figure 12 - Spanwise lift coefficient distributions c_l(y), trimmed cases, M = 0.